
Torque Estimation and Misfire Detection using Block Angular Acceleration

Jeffrey K. Ball and Martin J. Bowe
The United States Air Force Academy

C. Richard Stone and Peter D. McFadden
The University of Oxford

Reprinted From: **Modeling of SI Engines**
(SP-1511)

SAE routinely stocks printed papers for a period of three years following date of publication. Direct your orders to SAE Customer Sales and Satisfaction Department.

Quantity reprint rates can be obtained from the Customer Sales and Satisfaction Department.

To request permission to reprint a technical paper or permission to use copyrighted SAE publications in other works, contact the SAE Publications Group.



GLOBAL MOBILITY DATABASE

All SAE papers, standards, and selected books are abstracted and indexed in the Global Mobility Database

ISSN 0148-7191

Positions and opinions advanced in this paper are those of the author(s) and not necessarily those of SAE. The author is solely responsible for the content of the paper. A process is available by which discussions will be printed with the paper if it is published in SAE Transactions. For permission to publish this paper in full or in part, contact the SAE Publications Group.

Persons wishing to submit papers to be considered for presentation or publication through SAE should send the manuscript or a 300 word abstract of a proposed manuscript to: Secretary, Engineering Meetings Board, SAE.

Printed in USA

Torque Estimation and Misfire Detection using Block Angular Acceleration

Jeffrey K. Ball and Martin J. Bowe

The United States Air Force Academy

C. Richard Stone and Peter D. McFadden

The University of Oxford

ABSTRACT

This work examines the possibility of detecting misfires via measurements of the angular acceleration of the engine block. Measurements were taken on a production 4-cylinder engine which was modeled as a single degree of freedom torsional oscillator. The torque waveform was estimated and compared to the torque calculated via cylinder pressure measurements. Further analysis was conducted in the frequency domain. Results indicate that metrics based on low frequency information were most reliable, but this is impractical for vehicular applications. The accuracy of high frequency metrics was degraded due to the limitations of the model and the non-rigid behavior of the block at high engine speeds.

INTRODUCTION

Over the past several years, much effort has been placed into systems capable of detecting misfires in a spark-ignition engine. This interest was spawned by the California Air Resources Board (CARB) on-board diagnostic regulations for 1994 model year vehicles (OBD-II). According to the CARB regulations [1] engine misfire means, "lack of combustion in the cylinder due to absence of spark, poor fuel metering, poor compression, or any other cause". The regulations require that the vehicle's engine diagnostic system monitor misfire continuously. This concern is due to the fact that, even with a small number of misfiring cycles, engine performance degrades, hydrocarbon emissions increase, and driveability will suffer [2]. Furthermore, a misfired cycle results in a large quantity of unburned fuel being sent through the catalytic converter, which causes a reduction in its service life due to high temperature excursions [3]. Several methods of misfire detection have been proposed [3]:

a. Monitoring catalyst temperature. This method is unacceptable since the catalyst temperature does

not rise significantly in the case of low frequency misfire.

- b. Monitoring the oxygen sensor signal. This method also fails because a single misfire does not significantly alter the sensor output voltage.
- c. In-cylinder pressure monitoring. This method is the most accurate as individual cylinder IMEP could be calculated in real time. However, the cost of fitting each cylinder with a pressure transducer is prohibitive.
- d. Evaluation of crankshaft angular velocity fluctuations. This method has been the subject of much current work and appears to be very promising.

Method d) above is currently the most favored method of misfire detection. Whilst flywheel angular velocity fluctuations do provide good indices of misfire detection under certain engine operating conditions, one of the primary difficulties in implementing this method is the fluctuating load torque applied to the crankshaft through the drivetrain. The hypothesis in this work is that misfires can be detected by measuring the angular acceleration of the engine block, and that this measurement is relatively unaffected by the load applied at the opposite end of the drivetrain.

Examination of this hypothesis will begin with a review of the relevant literature pertaining to misfire detection by flywheel angular velocity measurements. This will be done in order to establish the current state of the art in misfire detection. A brief description of the experimental facilities used will be presented, followed by the development of the model used to reconstruct the torque applied by the cylinders in the engine. Next, various parameters will be derived for misfire detection, and the results of their use on a production 4-cylinder engine will be presented. The work will finally draw conclusions as to the advantages and disadvantages of using block angular acceleration as a method of misfire detection.

LITERATURE REVIEW

Before launching into a review of individual studies, it is helpful to examine, in general terms, the different methods of using flywheel velocity measurements. A classification system similar to that used by Williams [4] will be used here, and the various methods will be distinguished by the following characteristics:

- a. Complexity of system model.
- b. Metric of misfire detection.
- c. Methods of analysis.
- d. Assumptions.

COMPLEXITY OF SYSTEM MODEL – The system models used range in complexity from the use of no model at all, to the use of a full dynamic model, which includes crankshaft torsional vibration, and the dynamics of the drivetrain. If no model is used at all, the analysis is performed on the measured velocity signal. This has the advantage of simplicity, but is limited to identifying misfires through pre-computed threshold levels or pattern recognition (discussed in the Metrics of Misfire Detection Subsection) since without a model, cylinder torque cannot be reconstructed.

Next in order of complexity are models which use a single “lumped” inertia for the engine and drivetrain, and assume a rigid crankshaft. These models allow a composite cylinder torque to be calculated. If the engine in question does not have overlapping firing intervals, the torque signal can be temporally divided and the individual cylinder torques can be estimated. Such methods do not work well under conditions where either crankshaft torsional vibration or the fluctuating inertial properties of the engine are significant.

Finally, complex models have been used which incorporate a flexible crankshaft and include the dynamics of the drivetrain and engine. These models do allow the calculation of individual cylinder torque contributions in engines where the firing pulses do not overlap.

MISFIRE DETECTION METRICS – The parameter used to indicate a misfire is to a large degree dependent on the system model used in the analysis. In the case where no system model is used, one is forced into using either threshold criteria or pattern recognition to identify misfire. This requires the thresholds to be pre-computed for various speed and load combinations. Furthermore, threshold techniques can usually detect a misfire within an engine cycle, but may not be able to identify which cylinder misfired during that cycle. Pattern recognition techniques can allow identification of the specific misfiring cylinder, but at the added cost of collecting and computing reference patterns at various speed and load combinations.

For cases where a system model is employed, the reconstructed torque profile can be analyzed to identify misfire. The option still exists for using threshold criteria or pat-

tern recognition in this case. However, if the crankshaft is assumed to be rigid and the firing pulses do not overlap, the torque signal can be separated in the time (or crank angle) domain and the contribution of each individual cylinder can be calculated. Thus, the misfiring cylinder is immediately identified by a reduced contribution to the torque profile.

Several researchers have attempted to reconstruct cylinder pressure profiles from the flywheel angular velocity measurements. The major difficulty with this method is that the cylinder pressure has no effect on crankshaft torque (and hence flywheel angular velocity) at TDC. Hence, cylinder pressure cannot be reconstructed from the crankshaft torque at that point. Since the cylinder pressure at this point is critical to misfire detection, this limitation is a significant problem.

METHODS OF ANALYSIS – With the use of a system model, account must be made for the system response in calculating the torque applied to the crankshaft. This implies some sort of deconvolution in order to remove the effects of the reciprocating mass and to account for the system dynamics. Deconvolution in the frequency domain becomes an algebraic operation, hence, most of the researchers reviewed here perform their analysis in the frequency domain.

There are further advantages to analyzing the torque profile in the frequency domain. If the crankshaft is rigid and the firing pulses are uniform, the torsional excitation for all frequencies sums to zero except for multiples of the firing frequency (assuming each cylinder produces identical work on each firing pulse). In the case of a misfire, energy is transferred into sub-harmonics of the firing frequency, and this energy can be used to identify the misfire, normally through threshold values as outlined in the Metrics of Misfire Detection Subsection.

COMMON ASSUMPTIONS – Most researchers have assumed that the dynamics of the system are known and remain constant. At low engine speeds, this assumption is generally valid. However, the inertial properties of an engine are time-varying [5]. At higher engine speeds, the variation in inertial properties becomes more significant, with a resulting degradation in the accuracy of the model.

When analyzing the loads applied to the crankshaft, the load contributed by the drivetrain cannot be neglected. Normal procedure is to assume the drivetrain load is constant, and induces a DC torque to the crankshaft. This assumption should be valid in the case of an engine sitting in a test cell. However, for vehicular applications, significant dynamic loads can be induced in the drivetrain from the road.

The assumption of a torsionally rigid crankshaft has been mentioned numerous times in the preceding sections. The assumption is valid in cases where crankshaft torsional vibration is not significant, which means it is usually valid for low engine speeds. The torsional vibration characteristics of the crankshaft can be modeled, and

taken into account in the system model. However, complete elimination of the effects of crankshaft vibration requires independent velocity measurements at each crank throw, which at this time is not a feasible option.

Finally, most researchers assume non-overlapping firing pulses. This is required since only one measurement is taken. Hence, only a composite torque profile can be calculated. With this assumption, the composite torque can be temporally filtered in order to deduce each cylinder's contribution to the torque profile. This assumption is generally valid for engines with fewer than 8 cylinders [4].

REVIEW OF RELEVANT LITERATURE. – Citron et al. [6] developed a system for calculating engine torque and cylinder pressure from flywheel angular velocity measurements. They constructed a four degree of freedom model, which includes the crank and connecting rods, the flywheel, the vibration damper, and the vehicle loads (simulated by the dynamometer load). Each inertia is connected by torsional springs, and damping is included. The crankshaft was assumed to be rigid. The flywheel velocity was measured from the 142-tooth starter ring with a magnetic pick up. The velocity measurements were used as inputs to the model, and a crankshaft torque profile was calculated. This torque profile was assumed to be composed of a mean value plus a fluctuating component. They then subtracted the torque due to reciprocating components from this profile, and assumed that at TDC, the fluctuating component must be equal to the negative of the mean value (since cylinder torque at TDC is zero). The torque contribution for each cylinder was calculated by assuming that during the firing pulse, the firing cylinder was the only contributor to the torque profile. They also reconstructed cylinder pressure during the firing stroke for each cylinder, with the expected gaps in the calculations around TDC.

Plapp et al. [7] developed an engine roughness parameter based on the difference between successive angular accelerations of the flywheel; the angular acceleration calculated by differentiating the velocity measurements. Since the difference in angular acceleration is zero for constant speed or constant acceleration conditions, they conclude that the method is valid for steady-state and transient operation. They also used pattern recognition to discriminate between angular acceleration fluctuations produced by misfire and those produced by load inputs. Their method does not require a system model, although pre-calculations are required to establish pattern libraries.

Klenk et al. [3] also use the engine roughness parameter proposed by Plapp et al. [7] and a misfire threshold is pre-computed for various engine speed and load combinations. They accounted for road or driver induced transients by noting that a misfire would induce short term reductions in angular acceleration (and hence rotational energy) whilst transient operation (such as throttle lift-off) would induce a long term reduction in energy. The long-

term transients were then used to modify the threshold values or even, under extreme conditions, to disable the misfire detection system. It was found that the system worked best at low engine speeds where the rigid crankshaft assumption was most valid.

lida et al. [8] developed a system model from which the IMEP for each cylinder is estimated. The IMEP as used by them is the integral of the torque profile over the firing interval for each cylinder. Their model incorporated estimations of the torque applied by the valve train, accessories, and internal friction. It was found that at higher engine speeds, the model results were degraded due to crankshaft torsional vibration.

Brown and Neill [9] estimate cylinder pressure from flywheel angular velocity measurements by using reference patterns contained in a knowledge database. The method was employed on a Detroit Diesel V-6 engine. They recorded data at an operating speed of 1200 RPM, and varied the fuelling level in each cylinder. The crankshaft velocity fluctuations were recorded as each cylinder was under-fuelled to establish the reference pattern. These reference patterns were then used to predict maximum cylinder pressure in later tests with a claimed accuracy of $\pm 6\%$.

Several researchers have focused on calculating the indicated torque waveform in the frequency domain ([2], [10], [11], [12]). The method employed uses a rigid crankshaft, lumped inertial model for the system, and the load torque and friction torque are assumed constant. The applied torque on a crankshaft is thus given by [11]

$$T_c = T_p + T_m + T_f + T_L \quad (1)$$

where

- T_c = composite torque applied to crankshaft,
- T_p = torque due to gas pressure,
- T_m = torque due to reciprocating mass,
- T_f = torque due to friction load and pumping, and
- T_L = load torque through drivetrain.

Furthermore, the composite torque can be calculated through state-space deconvolution if the impulse response of the system is known. The angular velocity is related to the composite torque by [11]

$$\Omega(\theta) = \int_{-\infty}^{\theta} T_c(\gamma) h(\theta - \gamma) d\gamma \quad (2)$$

where $h(\theta)$ represents the impulse response of the system in the crank angle domain. When deconvolution is performed in the frequency domain, it becomes an algebraic operation, and the relationship between angular velocity and composite torque may be expressed by

$$T_c(\lambda_f) = \Omega(\lambda_f) H^{-1}(\lambda_f). \quad (3)$$

where $T_c(\lambda_f)$, $\Omega(\lambda_f)$, and $H^{-1}(\lambda_f)$ are the Fourier Transforms of the composite torque, angular velocity signal, and impulse response at the frequencies $n\lambda_f$, (or the harmonics of the firing frequency, λ_f). The reciprocating components also contribute energy to the harmonics of the firing frequency, and their contribution can be subtracted from the Fourier Transform of the composite torque to produce an indicated torque spectrum

$$T_i(\lambda_f) = T_c(\lambda_f) - T_r(\lambda_f) \quad (4)$$

where $T_r(\lambda_f)$ is the Fourier Transform of the torque due to the reciprocating mass at the engine firing frequencies. The torque due to reciprocating mass is entirely defined by engine geometry and speed, hence it can be pre-computed for various engine speeds. The contribution of the load and friction torque is neglected since they are assumed to be insignificant at the frequencies of interest. The advantage of the method outlined is that in the λ domain, the engine firing frequency is constant for a given engine regardless of engine speed [11]. The corresponding time-based frequencies are not. Furthermore, due to the periodic nature of engine combustion, harmonics of the firing frequency provide a better signal-to-noise ratio [2].

From equation (4), the resulting indicated torque waveform ($T_i(\lambda)$) represents the fluctuating torque component of the measured signal. This component is then used with various metrics to identify misfire. Lee and Rizzoni [2] calculate a torque vector for each engine cycle (one vector component for each cylinder). The torque vector components are defined as the rms value of the fluctuating torque in the harmonics deemed to be significant. These values are compared to the mean torque in order to identify a misfire. Connolly and Rizzoni [12] calculate an rms torque value for each cylinder in a cycle based on the energy contained in the first 3 harmonics of firing frequency, and develop probability density functions to define misfires.

Lee and Rizzoni [2] examine several different metrics for identifying misfire from the indicated torque waveform of equation (4). The first metric was a torque non-uniformity metric (TNM) and was based on the rms torque of each cylinder (incorporating an unspecified number of harmonics). The rms torque was subtracted from the mean torque to compute the TNM. The energy from torque non-uniformity (ETN) was based on the indicated torque waveform for an entire engine cycle. This had the effect of providing more data points for the Fourier Transform, with the result that the components of the torque signal below firing frequency could be analyzed. Since the energy contained in the sub-harmonics would theoretically be zero for identical cylinder combustion, a high level of energy at these frequencies would indicate a misfire. They also calculated a velocity non-uniformity metric (VNM) and an energy from velocity non-uniformity metric (EVN). These metrics were deduced from the measured

velocity signal directly, and were then computed in the same manner as the TNM and ETN metrics. The advantage here is in bypassing the requirement for a model and any inherent inaccuracies therein. Their results indicated that the energy based metrics (ETN and EVN) provided better indications of misfire than the non-uniformity metrics (TNM and VNM).

SUMMARY – This review has highlighted the significant features in work on detecting misfires via flywheel angular velocity fluctuations. The primary difficulties with this method are the assumptions of a rigid crankshaft and constant load torque. Thus, the hypothesis in this paper is that measurements of the angular acceleration of the engine block could be used in a manner similar to the methods reviewed here in order to detect misfires. It is assumed that the engine block can be more realistically considered to be rigid. Also, the load torque from the opposite end of the drivetrain should have a smaller effect on the response of the block at the frequencies of interest. Hence, it is hoped this method will overcome some of the disadvantages associated with crankshaft-based analysis.

The examination is presented in two stages. First, a model of the engine block is developed to include the requisite torque components and the stiffness and damping of the engine mounts. From this model, a torque waveform is calculated and compared to the torque produced by the cylinder gas pressure. Next, the torque and acceleration signals are analyzed in the spatial frequency domain. Metrics are developed from the information contained in the frequency analysis, and are then used to detect misfires. Finally, conclusions regarding the feasibility of the method in question will be discussed.

SYSTEM MODEL

The engine block was assumed to be rigid, and as a result was modeled as a single degree of freedom, damped torsional oscillator. A schematic of the engine model and axis system used is shown in Figure 1. The torsional stiffness and damping were provided by the engine mounts, and estimation of their properties will be discussed in the next section. Under these assumptions, the equation of motion for the engine block is

$$J_b \alpha_b + C_t \omega_b + K_t \theta_b = T_c(\theta) \quad (5)$$

where T_c is the composite torque applied to the block, and α_b , ω_b , and θ_b are the angular acceleration, velocity, and displacement of the engine block respectively. It must also be noted that there are two angular measurements involved in the model, namely crankshaft rotation and engine block rotation. The two measurements are distinguished by the subscript "b" which denotes rotation of the engine block. One would expect that the torque applied to the engine block would be equal and opposite to that applied to the crankshaft. However, this is not the

case (see Appendix A). The composite torque acting on the engine block thus becomes

$$T_c(\theta) = -T_p(\theta) - T_m(\theta) - T_f(\theta) + T'_m(\theta) \quad (6)$$

where

$T_p(\theta)$ = torque due to gas pressure,

$T_m(\theta)$ = torque due to reciprocating mass,

$T_f(\theta)$ = torque due to friction load and pumping, and

$T'_m(\theta)$ = correction to torque due to angular motion of the conrod.

Each of these terms are calculated as a function of *crankshaft* position. The derivation of each term in equation (6) is extensively covered by Taylor [13]. The details of this derivation are contained in Appendix A, and only the final expressions will be given here. The terms on the right hand side of equation (6) are given by

$$T_p(\theta) = P_{cyl} A_p \frac{\dot{Z}(\theta)}{\Omega} \quad (7)$$

$$T_m(\theta) = -M_p \ddot{Z}(\theta) \left(\frac{\dot{Z}(\theta)}{\Omega} \right) \quad (8)$$

$$T_f(\theta) = \frac{FMEP * V_d}{4\pi} \quad (9)$$

$$T'_m(\theta) = (J_{cr} - M_{cr} r_1 r_2) \Omega^2 \sum_{n=1}^{\infty} S_n \sin 2n\theta \quad (10)$$

where

P_{cyl} = measured cylinder pressure (N/m²),

A_p = piston area (m²),

Ω = engine angular velocity (rad/sec),

$\dot{Z}(\theta), \ddot{Z}(\theta)$ = instantaneous piston velocity and acceleration (m/sec, m/sec²),

FMEP = friction mean effective pressure (N/m²),

V_d = engine displacement (m³),

J_{cr} = moment of inertia of the conrod about its c.g. (kg-m²),

M_{cr} = mass of the conrod (kg),

r_1, r_2 = distances from conrod c.g. to centers of big and little ends (m), and

S_n = Fourier coefficients.

By combining equations (5) and (6), the torque due to gas pressure can be calculated by

$$-T_p(\theta) = J_b \alpha_b + C_t \omega_b + K_t \theta_b + T_m(\theta) + T_f(\theta) - T'_m(\theta). \quad (11)$$

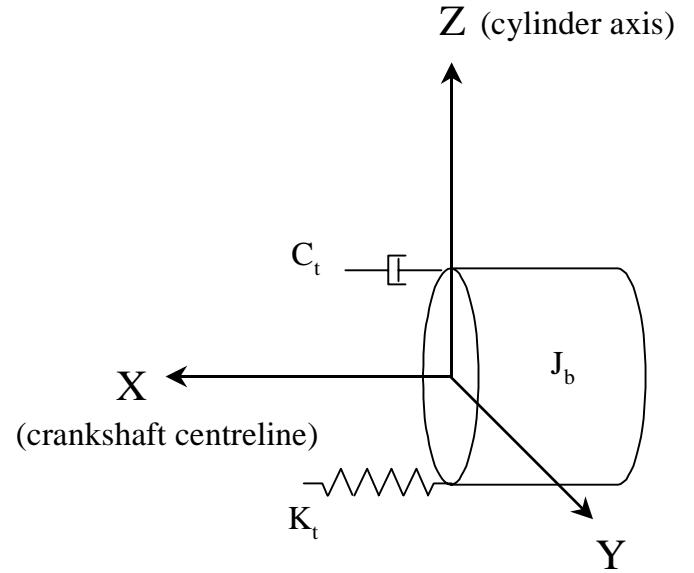


Figure 1. Single degree of freedom model.

The inertial properties of the engine were known, and the angular acceleration was measured. The angular velocity and displacement of the block were calculated by integrating the angular acceleration signal. The constants of integration were determined by assuming that the mean angular velocity and displacement must be zero over an engine cycle since the block did not wind up. The stiffness and damping coefficients were determined experimentally as described in the next section. Thus, the only "unknown" term in equation (11) was the torque due to gas pressure. However, the #4 cylinder contained a piezoelectric pressure transducer. Hence the torque due to gas pressure could be calculated for that cylinder. If all cylinders were assumed to have the same pressure-time histories, a composite gas pressure torque curve could be constructed to compare with the torque estimated by the angular acceleration measurements. Results of this comparison will be given later.

EXPERIMENTAL APPARATUS

The experimental work for this paper was performed on a Rover K series 4-cylinder petrol engine. The engine characteristics, including the mass properties, are shown in Table 1.

Table 1. Rover K16 specifications

| | |
|--------------------------------------|------------|
| Bore (mm) | 75 |
| Stroke (mm) | 79 |
| Displacement (liters) | 1.4 |
| Firing order | 1, 3, 4, 2 |
| Mass (kg) | 100 |
| I_x^1 (kg-m ²) | 4.75 |
| Conrod length (mm) | 121.3 |
| I_{cr}^2 (kg-m ²) | 0.477 |
| r_1^3 (mm) | 29.0 |
| r_2^4 (mm) | 92.3 |
| Piston mass (kg) ⁵ | .373 |
| Reciprocating mass (kg) ⁶ | .487 |

Notes:

1. Moment of inertia of the block about crankshaft centerline (see Figure 1).
2. Moment of inertia of conrod about center of gravity.
3. Distance from center of big end to center of gravity of conrod.
4. Distance from center of little end to center of gravity of conrod.
5. Piston mass includes mass of gudgeon pin.
6. Reciprocating mass assumes portion of conrod mass moves with piston (see Appendix A for derivation).

The K16 was instrumented with a Kistler type 6123 piezo-electric pressure transducer in the #4 cylinder connected to a Kistler 5007 charge amplifier. Two Bruel and Kjaer type 4382 piezo-electric accelerometers were mounted to the engine back plate as shown in Figure 2, with a spacing between accelerometers of 355 mm. The accelerometers were also connected to Kistler type 5001 charge amplifiers.

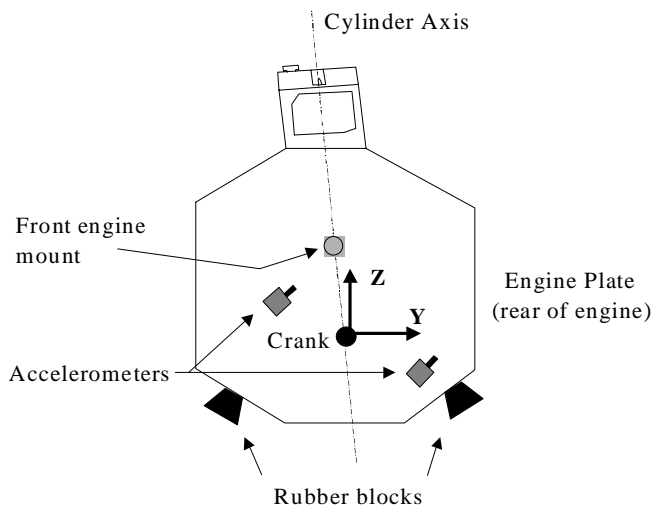


Figure 2. K16 engine mounts and accelerometer location.

The signals from the pressure transducer, accelerometers, and shaft encoder (TDC marker) were collected on the ComputerScope data acquisition system. The accel-

erometer signals were calibrated in units of m/sec², and the two signals were subtracted to remove any translational displacement component. The difference between the accelerometer signals was divided by the distance between the two accelerometers to calculate the angular acceleration of the block.

The engine mount stiffness was estimated by applying a couple of known magnitude to the engine frame (via weights and a spring scale) and measuring the angular displacement with a clinometer. The results of this experiment are shown in Table 2.

Table 2. Engine mount stiffness measurements.

| m_A (kg) | F_A (N) | F_B (N) | ΔT (N-m) | $\Delta\theta$ (minutes) |
|------------|-----------|-----------|------------------|--------------------------|
| 0.0 | 0.0 | 0.0 | 0.0 | 0.0 |
| 2.5 | 24.52 | 24.52 | 49.4 | 11 |
| 5.0 | 49.03 | 49.03 | 49.4 | 9 |
| 7.5 | 73.55 | 73.55 | 49.4 | 10 |
| 10.0 | 98.07 | 98.07 | 49.4 | 8 |
| 7.5 | 73.55 | 73.55 | 49.4 | 10 |
| 5.0 | 49.03 | 49.03 | 49.4 | 7 |
| 2.5 | 24.52 | 24.52 | 49.4 | 9 |
| 0.0 | 0.0 | 0.0 | 49.4 | 11 |
| Average | | | 49.4 | 9.4 |

The results of this experiment yielded an average torsional stiffness of 18,100 N-m/rad for the engine mounts. The damping coefficient was estimated by subjecting the engine block to an impulse and recording the angular acceleration, the results of which are shown in Figure 3.

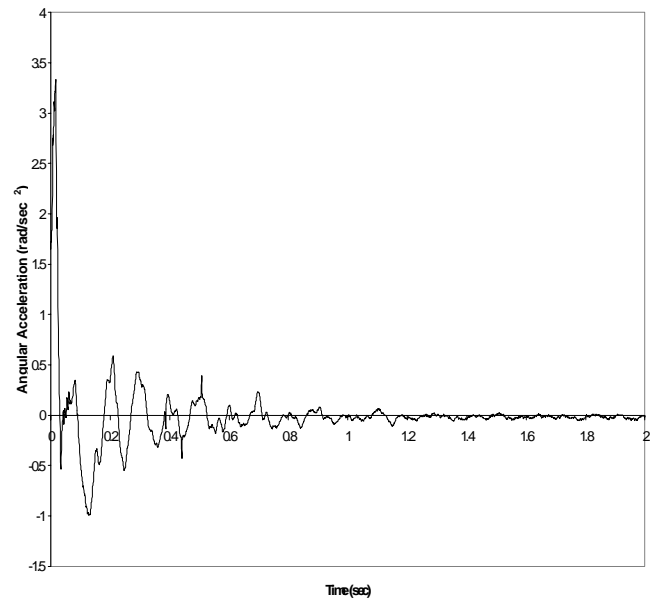


Figure 3. Impulse response of engine block.

The logarithmic decrement method of estimating the damping ratio is outlined in Thomson [14]. The analysis produced a damping ratio of $\zeta = 0.170$, and a torsional damping coefficient of $C_t = 99.7$ kg-m²/sec.

As a check on the calculated engine mount properties, a Discrete Fourier Transform (DFT) was performed on the impulse response shown in Figure 3. Furthermore, since the engine was modeled as a single degree of freedom oscillator, the non-dimensional magnitude of the impulse response in the frequency domain can be calculated by [14]

$$|H(f)| = \frac{1}{\sqrt{\left(1 - \left(\frac{f}{f_n}\right)^2\right)^2 + \left(2\zeta\left(\frac{f}{f_n}\right)\right)^2}} \quad (12)$$

where f_n is the undamped natural frequency of the oscillator, and is given by

$$f_n = \frac{1}{2\pi} \sqrt{\frac{K_t}{J_b}}. \quad (13)$$

The frequency response calculated by equation (12) is compared to the experimental frequency response in Figure 4.

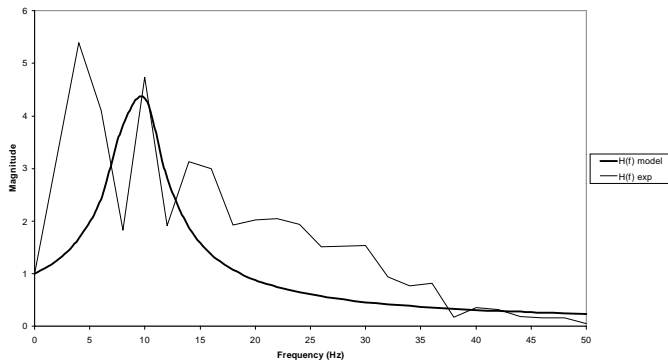


Figure 4. Comparison of experimental frequency response to model frequency response.

Several points must be brought out from Figure 4. First, the calculated stiffness properties predict a resonant torsional frequency of 9.83 Hz. This matches well with the experimental frequency response which shows a resonance peak at 10 Hz. However, the experiment also shows a resonance peak at 4 Hz. It is postulated that this resonance is due to a coupling between the torsional motion of the engine and the “pitching” motion (rotation about the Y-axis). There are two qualitative arguments for this. First, as the engine is run up on the dynamometer, a large resonance is experienced passing 240 RPM (a rotational frequency of 4 Hz). If the engine speed is held at 240 Hz, the engine can be seen to be visibly rocking about the Y-axis. Second, during the measurements of torsional stiffness, it was noted that at very large values of applied torque, the engine rotation was not purely about the X-axis. As the torque was applied purely in the

Y-Z plane, the off-axis rotation (again about the Y-axis) can be attributed to the location of the engine mounts. If the mounts were located in such a way that the suspension forces produced by them acted through the engine center of gravity, and the suspension couples produced by them acted about the principal axes of the engine, then the system would be decoupled [13]. This means that a force applied along an engine axis would only induce motion along that axis. Likewise, any torque applied around an axis would excite motion only about that axis. The current mounts on the K16 do not act through the c.g. or about any principal axis. What this implies is that the “rolling” and “pitching” motions of the engine block are both elastically and inertially coupled. Thus, a better model would incorporate two degrees of freedom, and a set of matrix equations would be solved to deduce the applied torque (this would also require the use of another set of accelerometers to measure the angular acceleration about the Y-axis). Since the coupling has its greatest effect at frequencies well below the firing frequency of the engine, the current model was not modified to account for this. This decision will also be evaluated in the course of analysing the results.

Since one of the primary objectives of the study was to examine the feasibility of using block angular acceleration measurements to detect misfires, the engine control system was modified to allow operator induced misfires on cylinder #4.

EXPERIMENTAL RESULTS – TORQUE ESTIMATION

The model described in the System Model Section and Appendix A was used to calculate the torque produced by the cylinders. Since only cylinder #4 had a pressure transducer, it was assumed that the other three cylinders had identical pressure histories to cylinder #4. This allowed a composite torque to be calculated from the gas pressure measurements, and was then used as a basis of comparison for the modeled torque. Data was collected for 360 consecutive cycles at the operating conditions shown in Table 3.

Table 3. Experimental operating points for Rover K16 engine.

| Case ID | Mot1 | W1010 | P1020 | Mot2 | 25115 | 25130 |
|----------------------------|-------|-------|-------|-------|-------|-------|
| Engine speed (RPM) | 1200 | 1200 | 1200 | 2500 | 2500 | 2500 |
| BMEP (bar) | -1.36 | 8.53 | 5.74 | -1.75 | 9.76 | 4.85 |
| λ | N/A | 1.0 | 1.0 | N/A | 1.0 | 1.0 |
| Ignition timing (deg BTDC) | N/A | 10 | 20 | N/A | 15 | 30 |

Two short sets of data (44 consecutive cycles) were taken whilst motoring the engine at each speed (Mot1 and Mot2). All firing tests were performed with gasoline as the fuel. The results are presented in the following figures, one figure for each engine speed. The figures show the engine torque as calculated by the angular acceleration model (denoted “Block measurements”) as a dotted line, and the engine torque calculated from the pressure measurements from cylinder #4 (denoted “Gas pressure”) as a heavy line. The composite gas torque curves were generated by assuming that the pressures in all cylinders were identical. Hence, the pressure in cylinder #4 was phased appropriately to calculate the torque produced by each cylinder.

Figure 5 indicates that at this engine speed (1200 RPM), the model does a reasonable job of estimating the cylinder torque. The model’s accuracy suffers somewhat at the WOT condition, where there appears to be a slight DC offset. This is most likely due to the friction correlation used in the model. The correlation given by the Rover Advanced Power Train Group (RAPT) is a function of engine speed only (see Appendix A), and this technique is supported by several others ([15], [16]). However, these correlations were derived from motored engines, and both the pumping and frictional losses tend to be under-estimated [17].

This indicates that friction correlations which account for the pressure load may give better results in this model, and such correlations have been proposed by Chen and Flynn [18] and Winterbone [19].

Another possible explanation for the decreased accuracy is the coupling between the rolling and pitching motion of the engine. Since the engine is of an in-line configuration, the effective moment arm for each cylinder about the Y-axis is different. It is expected that the pitching motion would be exacerbated at high load conditions (e.g., at wide-open throttle), and the model is not able to account for this effect. The results for 2500 RPM are shown in Figure 6.

The model’s accuracy is considerably less at this engine speed. Once again, the effect of the coupled rolling and pitching motion is seen at WOT. Furthermore, the accuracy is reduced even at part throttle operation. In this case, the cause is postulated to be the assumed inertial properties of the engine. The inertia of the engine varies during each rotation, but it is also a function of engine speed [5]. As a result, one would expect a model with constant inertial properties to perform better at low engine speeds, since normally the given inertial properties of an engine are calculated on a non-running engine. One would also expect that the effective moment of inertia at high engine speeds would be larger than that at low speeds. Thus, at high engine speeds, the inertial effects would be underestimated.

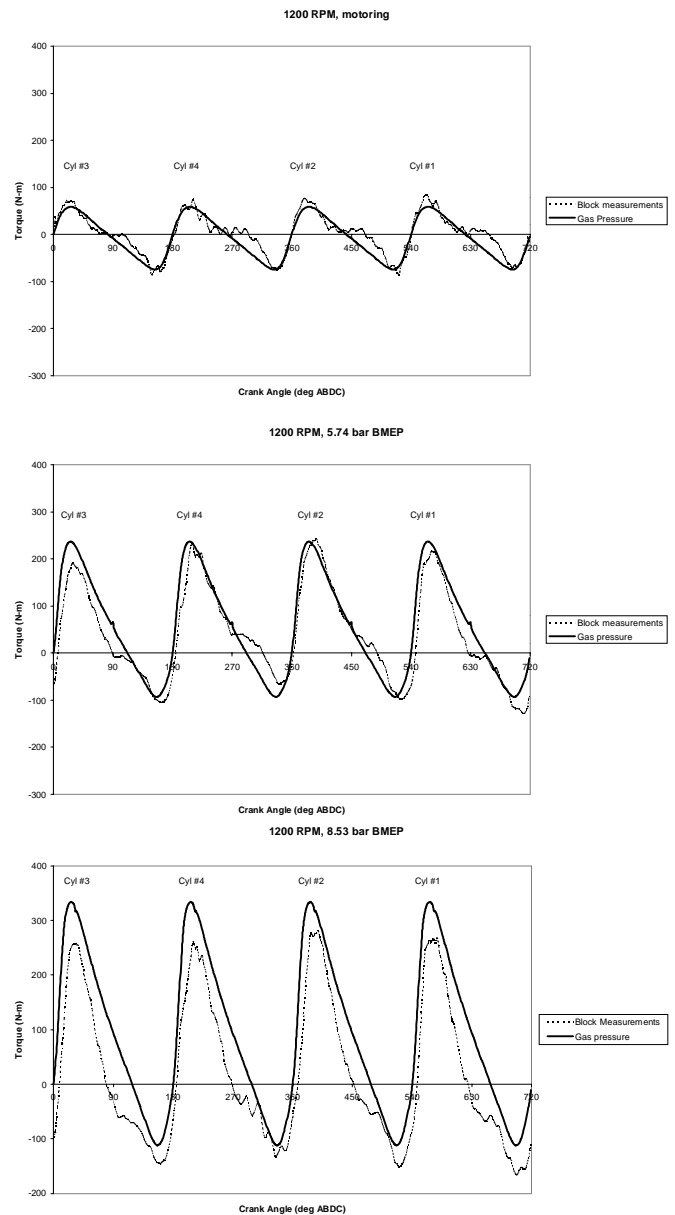


Figure 5. Comparison of torque calculated from angular acceleration of engine block to torque calculated from cylinder pressure measurements, 1200 RPM.

Another possible source of error is in the damping. It was assumed that the system contained viscous damping. However, rubber blocks do not in fact provide this type of damping. A better estimate may be given by assuming the mounts provide structural damping [20]. This type of damping is produced by the hysteresis effect shown by elastic materials undergoing cyclic loading. As such, it is roughly proportional to the square of the vibration amplitude, and is independent of frequency [20]. Overestimation of the damping would again lead to an underestimation of the torque.

Despite the limitations outlined, the current model will be examined as a means of misfire detection. The effective work done by the torque over one cycle is related to the mean effective pressure (MEP) by

$$\frac{4\pi T}{V_s} = \text{MEP} \quad (12)$$

This calculation can be performed over an entire engine cycle. However, this would not be of great value in detecting misfires. First, if only one misfire occurred during the cycle, the reduction in MEP would be very small since the other three cylinders would still be producing work (hence the value of multi-cylinder engines). Second, even if the reduction in MEP could be identified, it would only indicate a misfire had occurred, it would not identify the misfiring cylinder. However, the torque curve can be temporally divided in order to calculate the work done on the firing stroke of each individual cylinder (assuming non-overlapping firing intervals), and will be called the cylinder mean effective pressure (CMEP). Each cylinder's CMEP can be calculated and compared to the others within an engine cycle. If one of the cylinders had a low CMEP, it would be identified as the misfiring cylinder. Figure 7 shows a plot of CMEP for cylinder #4 versus the "IMEP" for that cylinder calculated over the firing stroke. Since the IMEP is negative for a misfired cycle, it gives a good indication of the ability of the CMEP to identify misfires.

Since the modeled torque curve at 1200 RPM was reasonable, one would expect good performance in misfire detection. The misfired cycles are clearly identified in Figure 7 by the fact that their IMEP is negative. The part load case in Figure 7 is ideal in that the CMEP is only negative for misfired cycles. Hence, in this case the misfires could be identified solely by cycles with a negative CMEP. In the WOT case, the misfired cycles could still be identified. However, the CMEP was negative for several cycles that had not actually misfired. This would require the use of some sort of threshold criteria to identify the misfired cycles, but the misfires could still be reliably detected. The cases at 2500 RPM are presented in Figure 8.

Given the inaccuracies in the calculated torque at this engine speed, the model would not be expected to provide a good misfire metric at this speed. There is no clear threshold value that could be selected that would enable the metric to detect the misfires in either case presented in Figure 8. The sources of error in this model were discussed previously, and further work should be done to examine whether the suggested model improvements might increase the accuracy of misfire detection at high speeds.

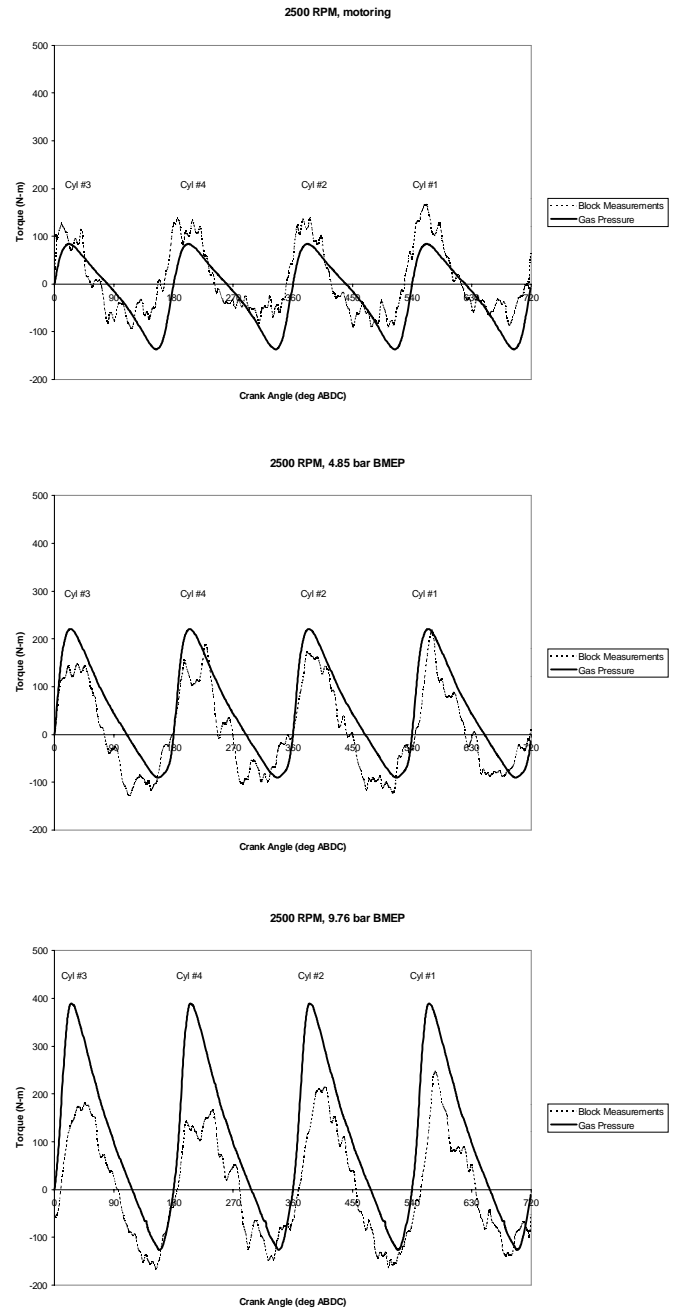


Figure 6. Comparison of torque calculated from angular acceleration of engine block to torque calculated from cylinder pressure measurements, 2500 RPM.

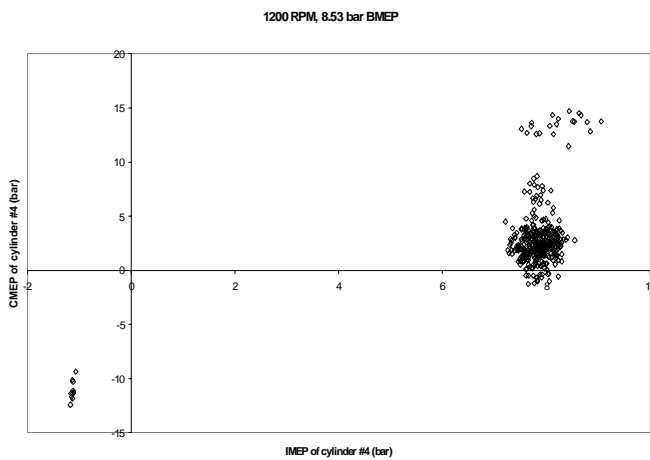
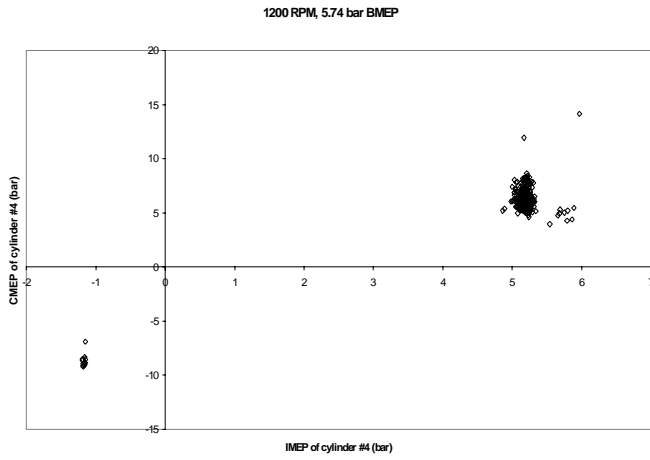


Figure 7. CMEP versus IMEP for cylinder #4, 1200 RPM.

Of course it is one matter to apply such a model to an engine sitting on a test bed, but quite another to apply it to an engine in an actual vehicle. The vehicle motion would significantly affect the angular acceleration measurements. Thus, the current metric (CMEP) might be of little value in a production vehicle. However, vehicle motion occurs at a frequency well below the firing frequency of the engine (ignoring for the moment any vibratory motion induced in the structure due to vehicular motion). Thus, the next portion of the work will attempt to analyze the calculated torque signal in the frequency domain, and to establish further metrics for misfire detection.

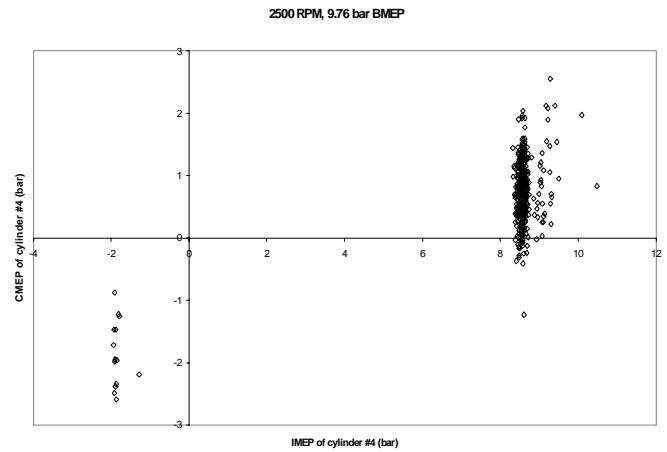
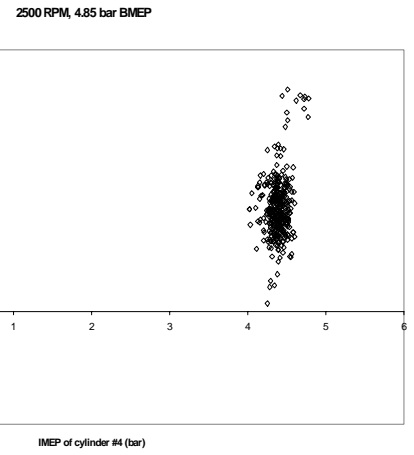


Figure 8. CMEP versus IMEP for cylinder #4, 2500 RPM.

EXPERIMENTAL RESULTS – FREQUENCY DOMAIN ANALYSIS

The frequency analysis will proceed in a manner similar to that outlined by Connolly and Rizzoni [12] and Lee and Rizzoni [2]. They have noted that frequency analysis of firing engine signals is best accomplished in the spatial frequency domain, where spatial frequency is defined as the Fourier Transform of the signal in the crankshaft angle domain. The advantage of this method is that in the crank-angle domain, the engine firing frequency (denoted λ_f) is independent of engine speed. Specifically, the K16 fires four times per engine cycle (one engine cycle being two revolutions) regardless of engine speed. This allows the analysis to be based on harmonics and sub-harmonics of the firing frequency, which should lead to a better signal-to-noise ratio [2].

The first step in the investigation was to perform Discrete Fourier Transforms (DFT's) on the experimental data. The results of the DFT's for the 1200 RPM, 5.74 bar BMEP case are presented in Figures 9 and 10. The DFT shown in Figure 9 was performed on blocks of data corresponding to one engine cycle, whilst the DFT of Figure 10 was performed on blocks of data corresponding to each cylinder's firing cycle. The former case provided a longer sample length and, since the sampling frequency was fixed at 180 samples/firing cycle, results in a finer frequency resolution on the plot. The DFT's in both figures were performed on cycles 18 and 19 of the data, cycle 19 being the first misfire in the data set.

The DFT in the top portion of Figure 9 was performed on the measured angular acceleration signal, whilst the lower figure was performed on the torque curve modeled as outlined in the System Model Section. Both cases indicate that a misfire tends to excite low orders in the engine block/mount system. The torque results show a large DC offset due to the misfire. This can be observed whilst the engine is running since a misfire causes the engine block to rotate significantly about its X-axis. The engine then requires 2-3 cycles to return to its equilibrium position. The acceleration results do not show an increase in DC offset. This would imply that the misfire acts as an impulse load, and whilst it does excite lower orders of acceleration, its duration relative to the engine cycle is too short to affect the mean acceleration value. Figure 10 repeats the analysis of Figure 9, except that the DFT was performed over blocks of data corresponding to each cylinder's firing cycle (180 data points). The same cycles were analyzed, and the results are for cylinder #4.

Figure 10 clearly illustrates the disadvantage of using a short sample length, namely, that some information is lost due to the decreased resolution of the frequency calculations. Nonetheless, there is still an increase in DC offset on the torque curve. There is also an increase in the DC offset on the acceleration curve. Again, it is postulated that this is due to the impulsive nature of the load imparted by the misfire. In the case presented in Figure 10, the DFT is performed over a shorter interval. Hence, the effect of the impulse is shown in the acceleration signal. This also has the effect of decreasing the magnitude in orders equal to and greater than the firing frequency.

Based on the aforementioned observations of the DFT results, four metrics of misfire detection were developed using techniques similar to those used by Lee and Rizzi [2] on the crankshaft angular velocity waveform. The first two are based on the DFT's of each engine cycle. Theoretically, if combustion were uniform, the frequency content in the range below the firing frequency would contribute no energy to the overall spectrum. Since the

frequency resolution in this case allows a closer examination of the magnitudes of the lower engine orders, the metric will be the energy contained in the orders below the firing order. The metric will be calculated on both the acceleration and torque signals. Thus, the Low Frequency Torque Metric (LFTM) is defined as

$$LFTM = \sqrt{\sum_{n=1}^{N-1} |T(n\lambda_o)|^2} \quad (14)$$

where $T(n\lambda_o)$ are the Fourier Transforms of the torque signal at frequencies below the firing order. Likewise, the Low Frequency Acceleration Metric (LFAM) is defined as

$$LFAM = \sqrt{\sum_{n=1}^{N-1} |A(n\lambda_o)|^2} \quad (15)$$

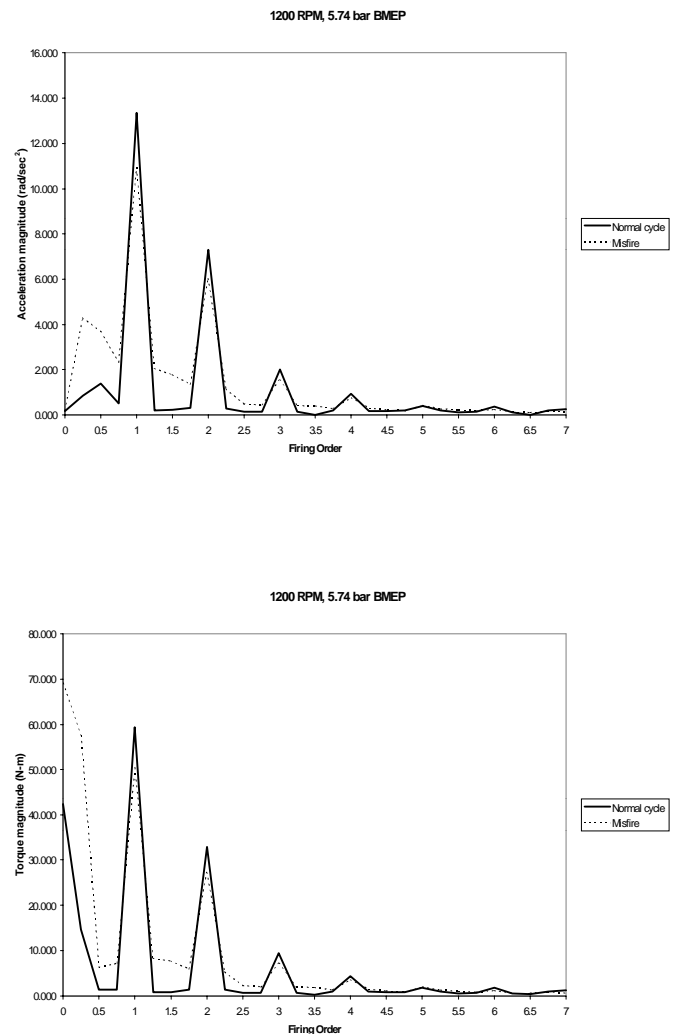


Figure 9. DFT of acceleration and torque waveforms, computed over entire engine cycle and comparing normal cycle to misfired cycle.

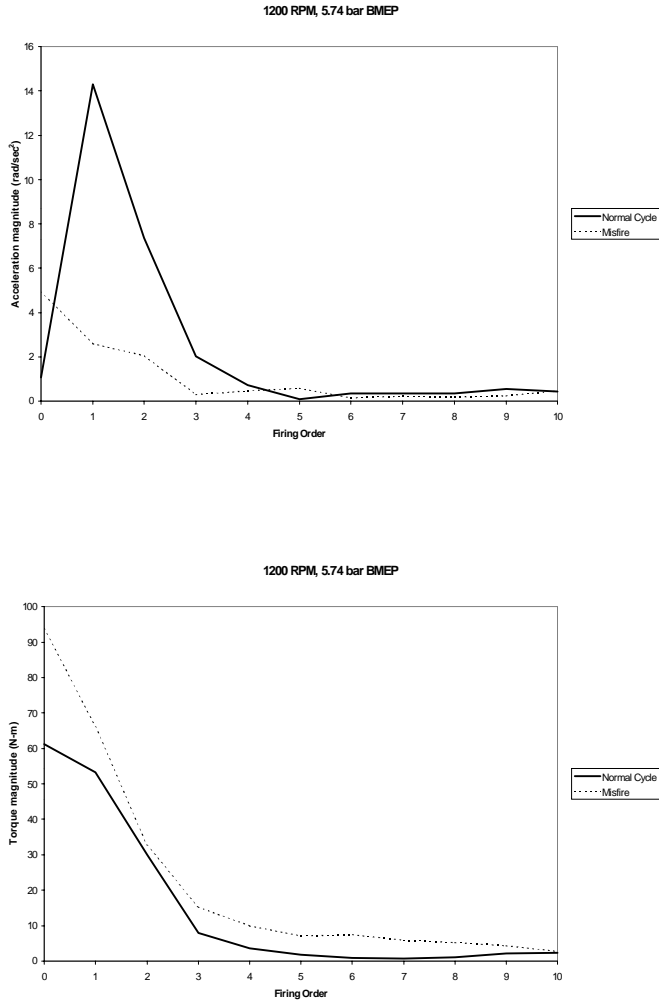


Figure 10. DFT of acceleration and torque waveforms, computed over firing cycle and comparing normal cycle to misfired cycle.

where $A(n\lambda_0)$ are the Fourier Transforms of the angular acceleration signal at frequencies below the firing order. These metrics are plotted against the IMEP of cylinder #4 in Figures 11 and 12 for the low speed, low load case and the high speed, high load case. Results for the other two cases are presented in Appendix B.

Figure 11 indicates that the LFTM could be used to identify misfires, although the high speed, low load case shown in Appendix B would result in a number of misidentified misfires (i.e., cycles identified as misfires which are not). However, once again the technique would require a threshold value to be set for each speed and load combination. Also, since the metric was calculated over each engine cycle, it can only be used to indicate that a misfire occurred on that cycle. It cannot distinguish which cylinder actually misfired. In the low speed, low load case presented in Figure 11, there are two points

which stand out from the right hand cluster. These two points are from cycles 166 and 167. In this case, the misfire circuit induced a double misfire on cycles 164 and 165. Hence, these two points show that a double misfire induces a larger DC offset on the block, and it then requires more cycles for this offset to return to the equilibrium position. The figure for the low speed, low load case (see Appendix B) also shows a separate cluster of points which correspond to cycles which follow a misfire. This indicates that it takes longer for the engine block to regain its equilibrium position after a misfire when the load is high. Intuitively this makes sense since at high loads, a misfire causes a greater impulse to be applied to the block and mounts, with a corresponding greater deflection. Figure 12 shows the results for the LFAM.

Once again, this metric could be used to identify misfires if appropriate threshold values were pre-computed. The effects of the double misfire are again noted in Figure 13 in the low speed case, where there is a high value of the LFTM for the cycle following the double misfire. Also, Figure B.2 of Appendix B shows the increased time required for the block to regain equilibrium after high load misfires.

The performance of the LFTM would tend to lead one to think the torque model used here was accurate at both high and low speeds. As explained previously, there are significant inaccuracies in the model at high engine speeds. However, the LFTM is largely influenced by the DC offset induced in the engine block due to a misfire. Even though the model does not accurately model the torque at high engine speeds, it still predicts the increase in DC offset. Since the errors primarily dominate at higher frequencies, this metric is able to overcome some of the limitations of the model in predicting misfires.

Although the previous metrics indicate a possibility of success in identifying misfires, their primary disadvantage is that they require low frequency information. This presents severe problems for an engine mounted in a vehicle, since vehicle motion could be expected to fall into the low-frequency category (relative to firing frequency). Thus, two more metrics were defined based on higher firing orders, and these used the results of the DFT's performed over the firing intervals for each cylinder. The metrics are estimates of the rms value of the individual cylinder torque and acceleration during one combustion period, and follow the procedure outlined by Lee and Rizzoni [2]. Thus, the High Frequency Torque Metric (HFTM) is defined as

$$HFTM = \frac{1}{L} \sqrt{\sum_{n=1}^L |T(n\lambda_f)|^2} \quad (16)$$

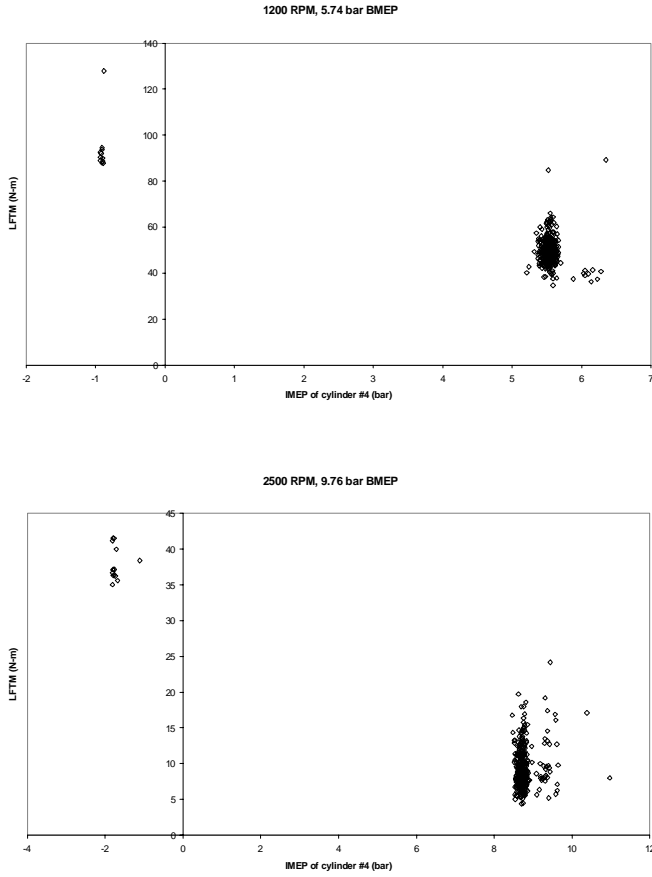


Figure 11. Low Frequency Torque Metric versus IMEP of cylinder #4.

where $T(n\lambda_f)$ are the Fourier Transforms of the torque signal at harmonics of the firing frequency. For this analysis, the first three harmonics were used. Likewise, the High Frequency Acceleration Metric (HFAM) is defined as

$$HFAM = \frac{1}{L} \sqrt{\sum_{n=1}^L |A(n\lambda_f)|^2} \quad (17)$$

where $A(n\lambda_f)$ are the Fourier Transforms of the angular acceleration signal at harmonics of the firing frequency. Results for the low speed, low load and high speed, high load cases are shown in Figures 13 and 14, the remaining cases are contained in Appendix B.

As might be expected after the discussion of the low frequency metrics, the HFTM would not be a reliable indicator of misfires. Some of the error in the HFTM is due to the previously discussed limitations of the model in calculating the torque. A further source of error is indicated by the work of Nakada and Tonosaki [21]. They investigated the vibrational characteristics of an in-line, 4-cylinder engine. They discovered that normal torque fluctuations (induced by cycle-by-cycle variation in combustion and the mass of reciprocating components) excited torsional vibration of the block at all orders and half orders of the engine rotation speed. Particularly, the second and fourth orders of rotation speed were strongly excited.

The second and fourth orders of engine rotation correspond to the first and second orders of firing frequency in a 4-cylinder engine. What this implies is that the assumption of a rigid block becomes less valid as engine speed increases. Thus, the rigid block assumption contains the same limitations as the rigid crankshaft assumption used by some of the work reviewed in the Literature Review Section. The limitations of assuming a rigid block are less apparent in the low frequency metrics due to the fact that misfires excite low orders very strongly. Hence, the errors associated with assuming a rigid block are overshadowed by the magnitude of the misfire-induced oscillations. Since the HFAM dispenses with the torque model altogether, it was hoped that it would be a more reliable indicator of misfire. The performance of the HFAM is shown in Figure 14.

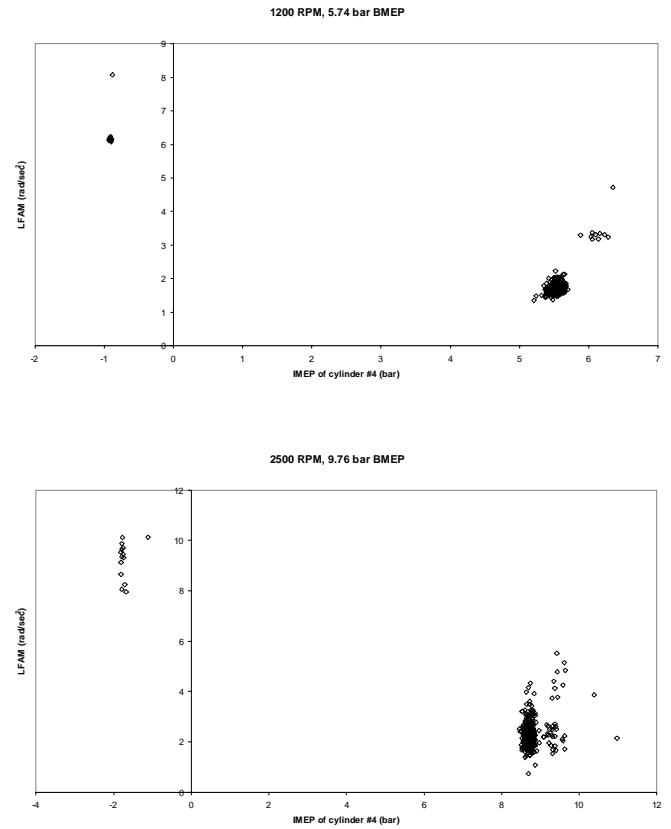


Figure 12. Low Frequency Acceleration Metric versus IMEP of cylinder #4.

The performance of the HFAM is very good at the low engine speed, but again suffers at higher engine speeds. Again, this is postulated to be due to the rigid block assumption. The HFAM does not use a model, hence it does not “account” for structural vibration of the block. Nevertheless, the vibrations are real and are present in the acceleration signal. As engine speed increases, the magnitude of the structural vibration due to reciprocating components increases. As a result, fluctuations in the acceleration signal due to cycle-by-cycle variation in combustion (or even complete misfires) are eventually

reduced to the level of noise in relation to the acceleration induced by the reciprocating mass. Thus, the signal itself is not sensitive enough to indicate the presence of a misfire. The solution to this problem is to develop a model that incorporates the structural vibration modes of the block, and to eliminate those modes from the calculated torque signal. This would enable an analysis of the torque fluctuations due to combustion alone, and should in theory increase the ability of the misfire detection metrics to identify misfires.

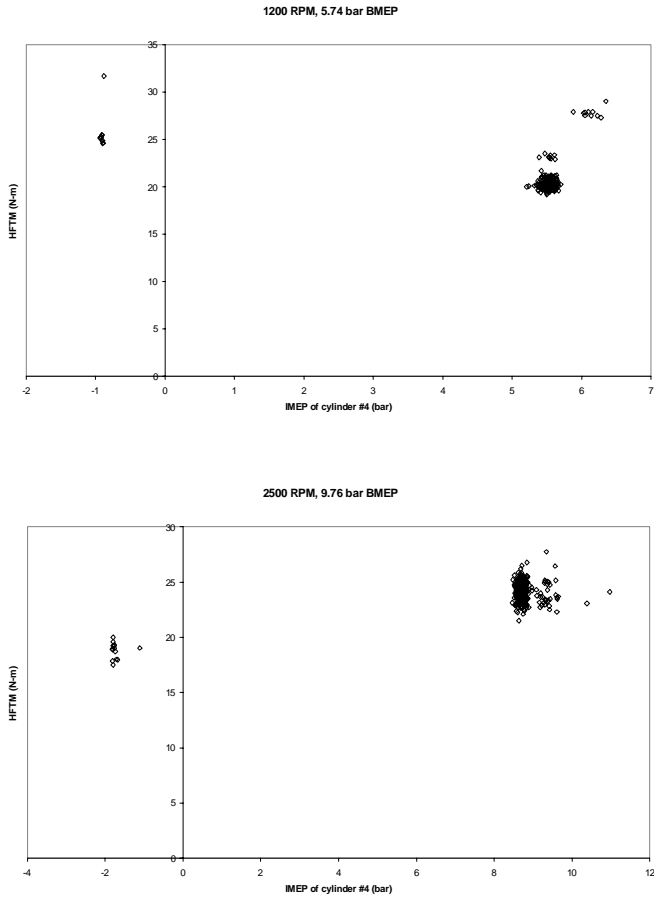


Figure 13. High Frequency Torque Metric versus IMEP of cylinder #4.

CONCLUSION

This work has focused on misfire detection by analyzing measurements of the angular acceleration of the engine block. Current practice is to use measurements of the flywheel angular velocity to detect misfires. This method is hampered by the load torque induced by the drivetrain, and torsional vibrations of the crankshaft. It was hypothesized that the method investigated here would overcome these limitations.

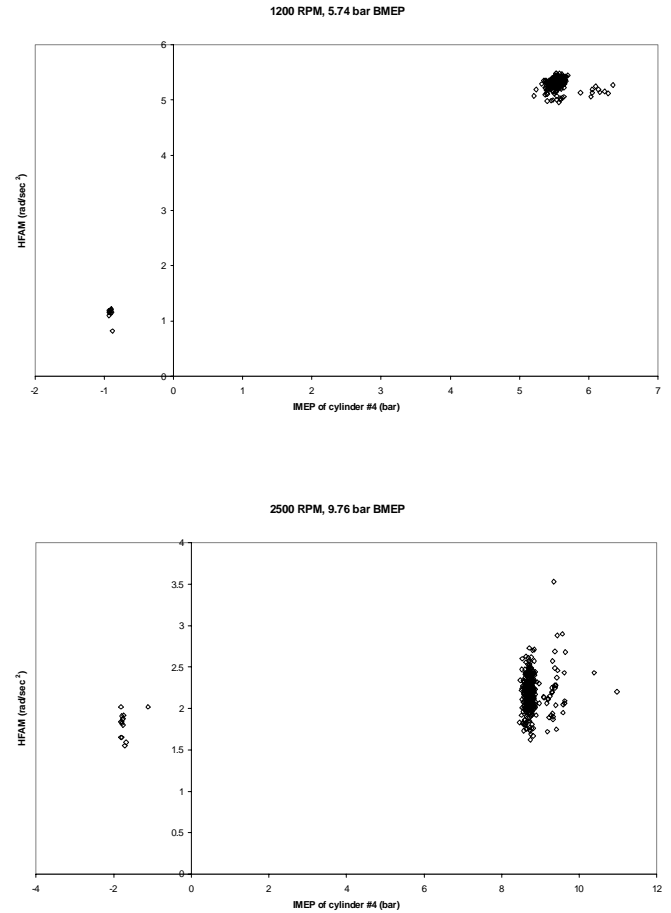


Figure 14. High Frequency Acceleration Metric versus IMEP of cylinder #4.

A model was constructed which assumed the block behaved as a single degree of freedom torsional oscillator. The calculated torque waveform confirmed that the angular acceleration of the block is not affected by the torque at the opposite end of the drivetrain. Furthermore, the calculated torque was reasonably accurate at low engine speeds and loads, but was not so accurate at higher engine speeds or loads. This was postulated to be due to coupling between the rolling and pitching motion of the engine block within its mounts. Nevertheless, the model was not affected by the load torque provided by the dynamometer.

The calculated torque waveform was then used to calculate a cylinder mean effective pressure (CMEP) for cylinder #4. This was compared to the IMEP for that cylinder on a cycle-by-cycle basis as a means of identifying misfires. It was found that the CMEP was a reliable indicator at lower engine speeds and loads. The inaccuracies in the CMEP at higher speeds and loads were assumed to be the result of the previously discussed limitations to the one degree of freedom model.

Next, both the torque waveform and the measured angular acceleration signal were analyzed in the spatial frequency domain. Four metrics for misfire identification were developed, based on either low or high frequency information. The results indicated that misfires tended to excite low orders in the engine block/mount system. Thus, metrics based on the energy contained in the low orders (below firing frequency) could be used to identify misfires.

The metrics based on the high frequency information were not generally reliable as misfire indicators. This is most likely to be due to the assumption of a rigid block. The block has been shown to undergo structural vibration at relatively low orders of firing frequency [21]. In the case of the metric using the acceleration signal, it is postulated that the magnitude of the structural vibrations at high engine speeds becomes so large as to mask the effects of the torque fluctuations. The metric based on the calculated torque waveform does not account for structural vibration at all, with predictable results.

The final conclusion from this portion of the work is that the method of using block angular acceleration measurements is a viable means of both torque estimation and misfire identification. The accuracy of the torque estimation would be improved by:

1. Including the rigid body pitching motion of the block as a second degree of freedom. (The rear mounts on the production K16 are actually incorporated into the gearbox. The effects of this location on the pitching motion of the engine need to be examined, since it may eliminate the need to account for the pitching motion.)
2. Including structural vibration of the block (elimination of the rigid block assumption).
3. Incorporating variable inertial properties of the block based on engine speed.

Currently, the most reliable indicators of misfire are based on low order frequency information. This presents severe problems for identifying misfire in an engine mounted in a vehicle. With a model incorporating the changes suggested above, it is anticipated that high frequency information would be available for misfire identification, thus making it more suitable for vehicular applications.

ACKNOWLEDGMENTS

Jeff Ball is grateful to the US Air Force and the Air Force Institute of Technology for sponsoring his studies at the University of Oxford. The authors are also grateful to Rover for their assistance and technical advice on the Rover K16 engine.

REFERENCES

1. California Air Resources Board (1991), *Technical status Update and Proposed Revisions to Malfunction and Diagnostic System Requirements Applicable to 1994 and Subsequent California Passenger Cars, Light-Duty Trucks, and Medium-Duty Vehicles – (OBDII)*, CARB staff report.
2. Lee, D., and Rizzoni, G. (1995), *Detection of Partial Misfire in IC Engines Using Measurement of Crankshaft Angular Velocity*, SAE Paper 951070.
3. Klenk, M., Moser, W., Mueller, W., and Wimmer, W. (1993), *Misfire Detection by Evaluating Crankshaft Speed – A Means to Comply with OBDII*, SAE Paper 93099.
4. Williams, J. (1996), *An Overview of Misfiring Cylinder Engine Diagnostic Techniques Based on Crankshaft Angular Velocity Measurements*, SAE Paper 960039.
5. Shiao, Y., and Moskwa, J.J. (1994), *Misfire Detection and Cylinder Pressure Reconstruction for SI Engines*, SAE Paper 940144
6. Citron, S.J., O'Higgins, J.E., and Chen, L. (1989), *Cylinder by Cylinder Engine Pressure and Pressure Torque Waveform Determination Utilizing Speed Fluctuations*, SAE Paper 890486.
7. Plapp, G., Klenk, M., and Moser, W. (1990), *Methods of On-Board Misfire Detection*, SAE Paper 900232.
8. Iida, K., Akishino, K., and Kido, K. (1990), *IMEP Estimation from Instantaneous Crankshaft Torque Variation*, SAE Paper 900617.
9. Brown, T.S., and Neill, W.S. (1992), *Determination of Engine Cylinder Pressures from Crankshaft Speed Fluctuations*, SAE Paper 920463.
10. Rizzoni, G. (1986), *A Dynamic Model for the Internal Combustion Engine*, PhD dissertation, University of Michigan, Ann Arbor, Mich.
11. Connolly, F.T. (1994), *Direct Estimation of Cyclic Combustion Pressure Variability using Engine Speed Fluctuations in an Internal Combustion Engine*, SAE Paper 940143.
12. Connolly, F.T., and Rizzoni, G. (1994), *Real Time Estimation of Engine Torque for the Detection of Engine Misfires*, Transactions of the ASME, Journal of Dynamic Systems, Measurement, and Control, Vol. 116, pp. 675-686.
13. Taylor, C.F. (1985), *The Internal Combustion Engine in Theory and Practice*, Volume 2, MIT Press, Cambridge, Massachusetts.
14. Thomson, W.T. (1988), *Theory of Vibration with Applications*, Prentice Hall, New Jersey.
15. Barnes-Moss, H.W. (1975), *A designer's viewpoint*, in Passenger Car Engines, ImechE Conf. Proc., pp.133-147, MEP, London.

16. Heywood, J.B. (1988), *Internal Combustion Engine Fundamentals*, McGraw-Hill Book Company, New York.
17. Stone, C.R. (1992), *Introduction to Internal Combustion Engines*, 2nd Edn. Macmillan.
18. Chen, S.K., and Flynn, P. (1965), *Development of a compression ignition research engine*, SAE Paper 650733.
19. Winterbone, D.E. (1986), 'Transient performance', in Horlock, J.H. and Winterbone, D.E. (eds), *The Thermodynamics and Gas Dynamics of Internal Combustion Engines*, Vol. II, Oxford University Press.
20. Meirovitch, L. (1975), *Elements of Vibration Analysis*, McGraw-Hill, Inc., New York.
21. Nakada, T., and Tonosaki, H. (1994), *Excitation Mechanism of Half Order Engine Vibrations*, Paper C487/017, Proceedings of the IMechE.

APPENDIX A DERIVATION OF COMPOSITE TORQUE USING ENGINE BLOCK ANGULAR ACCELERATION

The following derivation is contained in detail in Taylor [13]. Taylor develops expressions for the torque applied to the crankshaft, as this method is physically more intuitive. The signs may then be adjusted appropriately to apply the torque to the block, or engine frame to use Taylor's terminology. To begin, the composite torque acting on the crankshaft is

$$T_c = T_p + T_m + T_f + T'_m \quad (A.1)$$

where

- T_c = composite torque applied to the crankshaft,
- T_p = torque due to gas pressure,
- T_m = torque due to reciprocating mass,
- T_f = torque due to friction load and pumping, and
- T'_m = correction to torque due to angular motion of the conrod.

The axis system used for this derivation is shown in Figure A.1 below, and follows normal automotive practice.

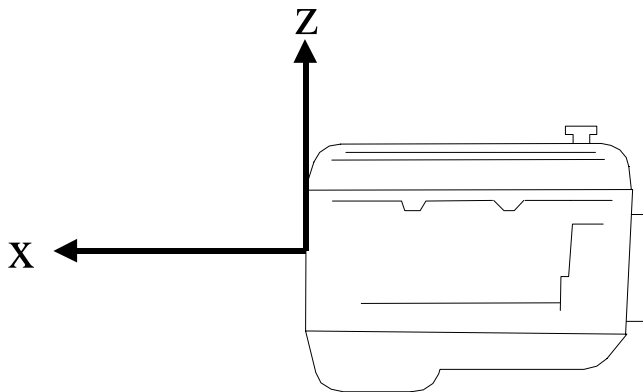


Figure A.1. Engine axis system.

With this axis system, a positive torque is in the direction of crankshaft rotation (clockwise as viewed from the front of the engine). The derivation starts by defining the position and motion of the piston as defined in Figure A.2.

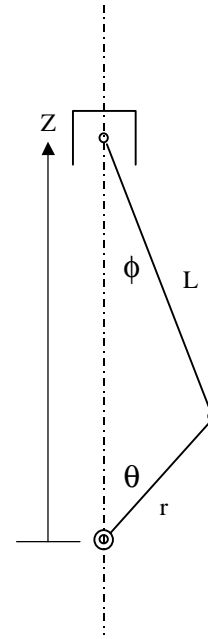


Figure A.2. Piston position.

The position of the little end with respect to the crankshaft center is

$$Z = L \cos \phi + r \cos \theta . \quad (A.2)$$

Since $L \sin \phi = r \sin \theta$, and $\cos^2 \phi + \sin^2 \phi = 1$, the position of the little end becomes

$$Z = r \left[\cos \theta + \frac{L}{r} \sqrt{1 - \left(\frac{r}{L} \right)^2 \sin^2 \theta} \right]. \quad (A.3)$$

The binomial theorem may be used to expand the radical

$$Z = r \left\{ \cos \theta + \frac{L}{r} \left[1 - \frac{1}{2} \left(\frac{r}{L} \right)^2 \sin^2 \theta - \frac{1}{8} \left(\frac{r}{L} \right)^4 \sin^4 \theta + \dots \right] \right\} \quad (A.4)$$

The powers of $\sin\theta$ can be expressed as equivalent multiple angles which produces

$$Z = r \left\{ \cos\theta + \frac{L}{r} \left[1 - \frac{1}{2} \left(\frac{r}{L} \right)^2 (1/2 - 1/2 \cos 2\theta) \right] \right\} + r \left\{ \cos\theta + \frac{L}{r} \left[-\frac{1}{8} \left(\frac{r}{L} \right)^4 (3/8 - 1/2 \cos 2\theta + 1/8 \cos 4\theta) + \dots \right] \right\} \quad (\text{A.5})$$

Normally, $(r/L)^2$ is less than 0.1, and the $(r/L)^4$ terms can be neglected. Thus

$$Z \approx r \left\{ \cos\theta + \frac{L}{r} \left[1 - \frac{1}{2} \left(\frac{r}{L} \right)^2 (1/2 - 1/2 \cos 2\theta) \right] \right\}. \quad (\text{A.6})$$

This expression can be differentiated twice to give the piston velocity and acceleration (assuming constant angular velocity of the crankshaft):

$$\dot{Z} \approx -r\Omega \left(\sin\theta + \frac{1}{2} \frac{r}{L} \sin 2\theta \right) \quad (\text{A.7})$$

$$\ddot{Z} \approx -r\Omega^2 \left(\cos\theta + \frac{r}{L} \cos 2\theta \right) \quad (\text{A.8})$$

The reciprocating mass contains the mass of the piston and gudgeon pin, plus some portion of the conrod mass. This is usually accomplished by treating the conrod as two masses as shown in Figure A.3.

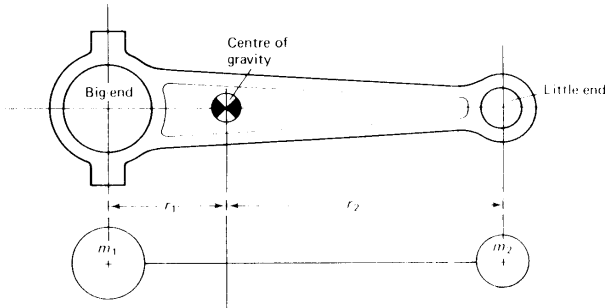


Figure A.3. Equivalent conrod mass (from Stone [17]).

For equivalence

$$m_{cr} = m_1 + m_2$$

$$m_1 r_1 = m_2 r_2.$$

The mass m_2 is considered to be part of the piston assembly, and is assumed to undergo reciprocating motion only. The mass m_1 is assumed to undergo pure rotation with the crankshaft, and is normally countered with balance weights incorporated into the crankshaft.

TORQUE APPLIED TO CRANKSHAFT DUE TO GAS PRESSURE

The torque due to gas pressure may be found by noting that the work done by the gas must be equal to the work done on the crankshaft

$$PdV = T_p d\theta. \quad (\text{A.9})$$

Since $dV = A_p dZ$, where A_p is the piston area,

$$T_p = PA_p \frac{dZ}{d\theta}. \quad (\text{A.10})$$

However,

$$\frac{dZ}{d\theta} = \frac{dZ/dt}{d\theta/dt} = \frac{\dot{Z}}{\Omega}. \quad (\text{A.11})$$

Therefore

$$T_p = PA_p \frac{\dot{Z}}{\Omega}. \quad (\text{A.12})$$

TORQUE APPLIED TO CRANKSHAFT DUE TO RECIPROCATING MASS

The torque applied to the crankshaft by the reciprocating mass is found by noting that the change in kinetic energy of the piston is equal to the work done by the crankshaft on the conrod

$$d \left(\frac{M_p}{2} \dot{Z}^2 \right) = -T_m d\theta. \quad (\text{A.13})$$

Differentiating equation (A.13) with respect to time gives

$$\frac{d}{dt} \left(\frac{M_p}{2} \dot{Z}^2 \right) = M_p \dot{Z} \ddot{Z} = -T_m \frac{d\theta}{dt} = -T_m \Omega. \quad (\text{A.14})$$

Finally

$$T_m = -M_p \dot{Z} \left(\frac{\dot{Z}}{\Omega} \right). \quad (\text{A.15})$$

CORRECTION TO TORQUE DUE TO ANGULAR MOMENTUM OF THE CONROD

The torque required to rotate the conrod may be determined by reference to Figure A.4.

The required torque is given by Newton's Law, and is $I_{cr} \ddot{\phi} = fL \cos \phi$, hence

$$f = \frac{I_{cr} \ddot{\phi}}{L \cos \phi} \quad (\text{A.16})$$

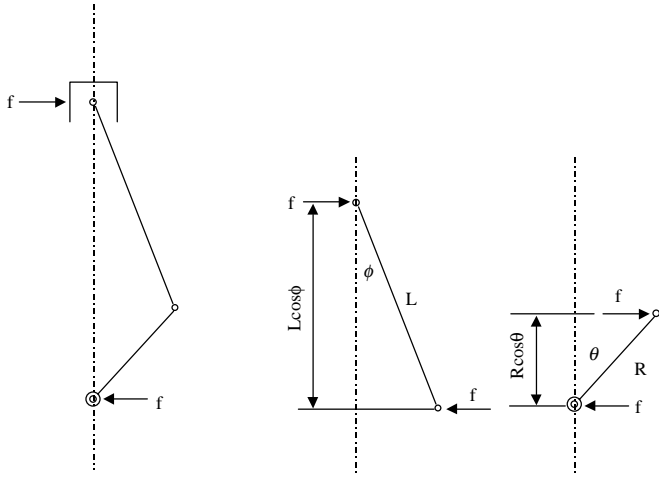


Figure A.4. Inertia torques acting on conrod and engine block (from Taylor [13]).

The torque acting on the crankshaft will thus be

$$T = fr \cos \theta = \frac{I_{cr} \ddot{\phi} r \cos \theta}{L \cos \phi}. \quad (\text{A.17})$$

The torque due to the reciprocating mass of the conrod has been accounted for in the derivation of T_m . However, the fictitious conrod used in this derivation has a different moment of inertia than the actual conrod, thus a correction must be applied to equation (A.1). The moment of inertia of the fictitious conrod is

$$I'_{cr} = (m_1 r_1^2 + m_2 r_2^2). \quad (\text{A.18})$$

From the equations used to establish the equivalency of the fictitious rod, $m_1 = m_2 r_2 / r_1$ and $m_2 = m_1 r_1 / r_2$. Making this substitution into equation (A.18) gives

$$I'_{cr} = M_{cr} r_1 r_2. \quad (\text{A.19})$$

In considering the torque required to rotate the conrod, the difference between the torque acting on the actual rod and that acting on the fictitious rod is

$$(I_{cr} - M_{cr} r_1 r_2) \ddot{\phi}. \quad (\text{A.20})$$

Combining equations (A.19) and (A.20) thus gives the correction to the inertia torque for the true moment of inertia of the conrod

$$T'_m = (I_{cr} - M_{cr} r_1 r_2) \ddot{\phi} \frac{r \cos \theta}{L \cos \phi}. \quad (\text{A.21})$$

With reference to Figure A.4, it can be seen that the correction to the inertia torque applied to the block is not equal and opposite to equation (A.21). In this case, the torque applied to the block is $f(r \cos \theta + L \cos \phi)$, and equation (A.21) becomes

$$T'_m = (I_{cr} - M_{cr} r_1 r_2) \ddot{\phi} \left(\frac{r \cos \theta}{L \cos \phi} + 1 \right). \quad (\text{A.22})$$

Equation (A.22) may be reduced to a trigonometric series (Taylor [13])

$$T'_m = (I_{cr} - M_{cr} r_1 r_2) \Omega^2 \sum_{n=1}^{\infty} S_n \sin 2n\theta \quad (\text{A.23})$$

where S_n are coefficients given by Taylor [13] to be -0.35 and -0.055 for the first two terms of the series.

TORQUE APPLIED TO CRANKSHAFT DUE TO FRICTION

Determining the friction level in an engine is a notoriously difficult task [17]. Often, a motoring test is performed with the assumption that the torque required to motor the engine is equal to the friction torque. However, the friction level will change under firing conditions due to the increased temperature of operation and the greater gas pressure loads within each cylinder. The engine used for this work is a four-cylinder Rover K16 1.4 liter MPI engine. The Rover Advanced Power Train division has developed an expression for the friction mean effective pressure (FMEP) for this engine, and this correlation has shown good agreement with experiment. The FMEP (in bar) may be estimated by

$$FMEP = 0.697 + N(2.995 \times 10^{-8} N - 1.487 \times 10^{-5}) \quad (\text{A.24})$$

where N is the engine speed in revolutions per minute. The torque due to friction is related to the FMEP by noting that the work done by the torque in two revolutions is equal to the MEP times the engine displacement [13]

$$T_f (4\pi) = FMEP * V_d. \quad (\text{A.25})$$

Hence, the torque due to friction is

$$T_f = \frac{FMEP * V_d}{4\pi} \quad (\text{A.26})$$

and this is assumed to be constant over the entire cycle.

The foregoing equations were derived for a single cylinder. Since all the torques act about the same axis, the torques produced by each cylinder may be added directly. This is accomplished by varying the phasing of each cylinder's torque input on the basis of engine firing order.

The composite torque acting on the engine block is not equal and opposite to the torque acting on the crankshaft due to the correction torque from the rotation of the conrod. However, a separate correction factor has been derived. Hence, the composite torque acting on the engine block is given by

$$T_c = -T_p - T_m - T_f + T'_m \quad (\text{A.27})$$

APPENDIX B MISFIRE METRIC RESULTS

The figures in this appendix plot the misfire identification metrics versus the IMEP of cylinder #4. The four metrics were defined as:

Low Frequency Torque Metric -
$$LFTM = \sqrt{\sum_{n=1}^{N-1} |T(n\lambda_o)|^2}$$

Low Frequency Acceleration Metric -

$$LFAM = \sqrt{\sum_{n=1}^{N-1} |A(n\lambda_o)|^2}$$

High Frequency Torque Metric -

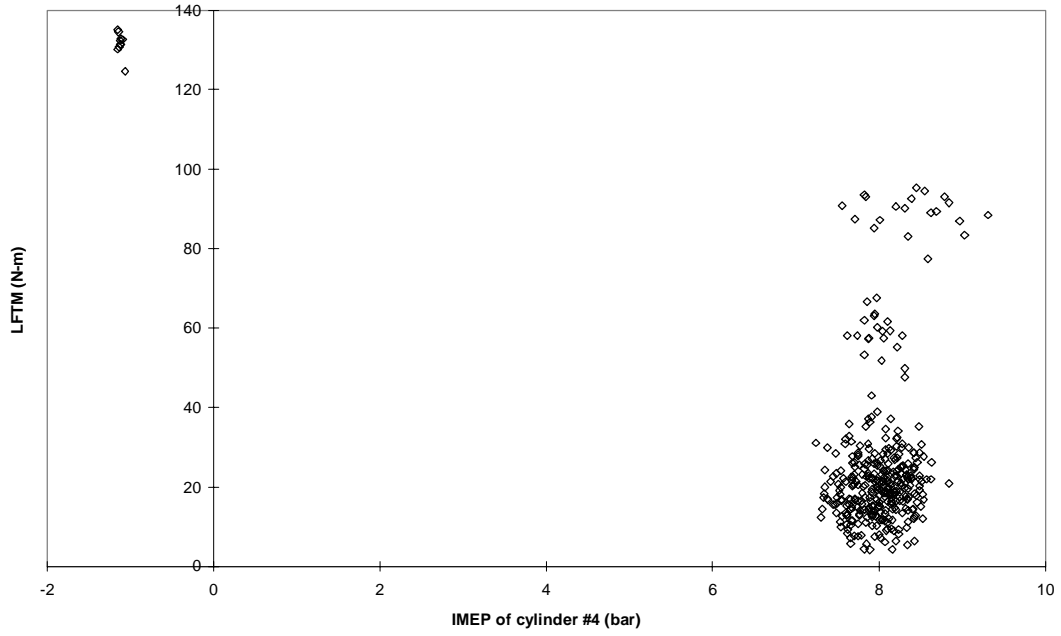
$$HFTM = \frac{1}{L} \sqrt{\sum_{n=1}^L |T(n\lambda_f)|^2}$$

High Frequency Acceleration Metric -

$$HFAM = \frac{1}{L} \sqrt{\sum_{n=1}^L |A(n\lambda_f)|^2}$$

The cases presented are the low speed, high load case and the high speed, low load case.

1200 RPM, 8.53 bar BMEP



2500 RPM, 4.85 bar BMEP

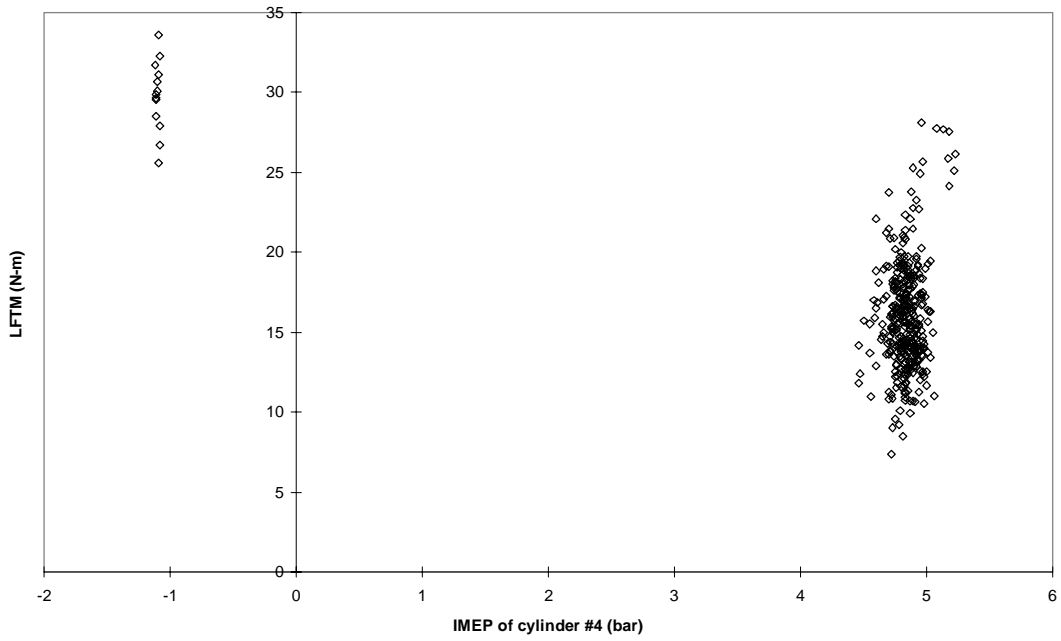
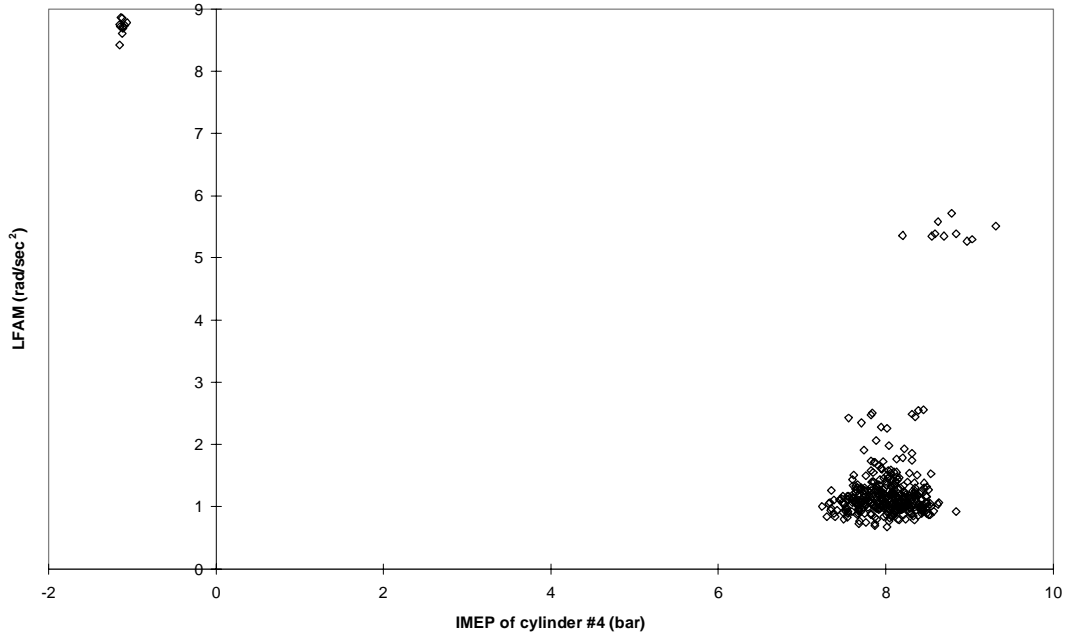


Figure B.1. LFTM versus IMEP of cylinder #4.

1200 RPM, 8.53 bar BMEP



2500 RPM, 4.85 bar BMEP

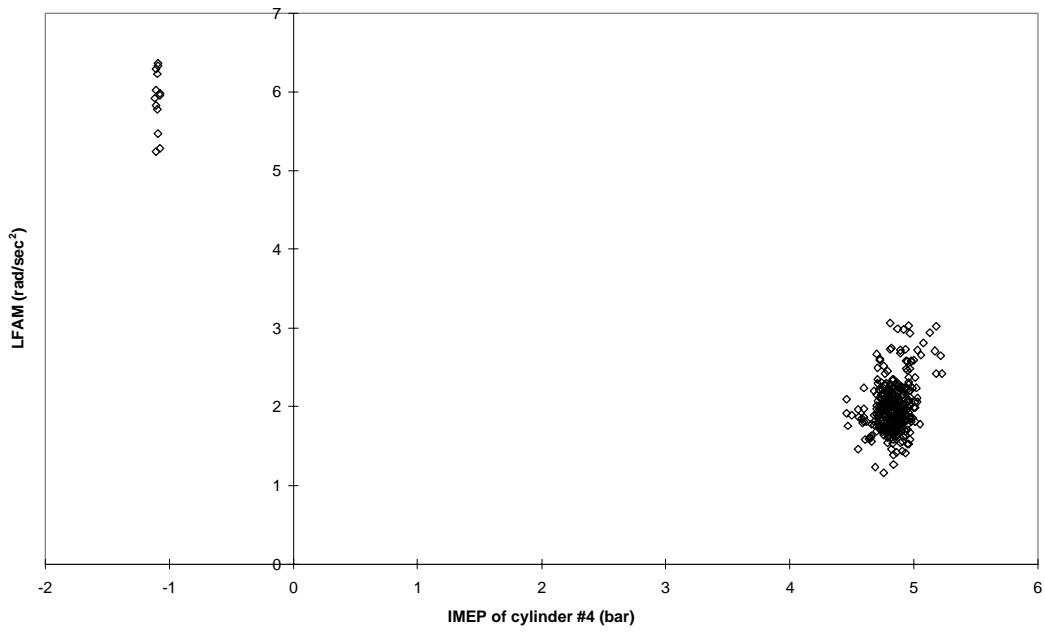
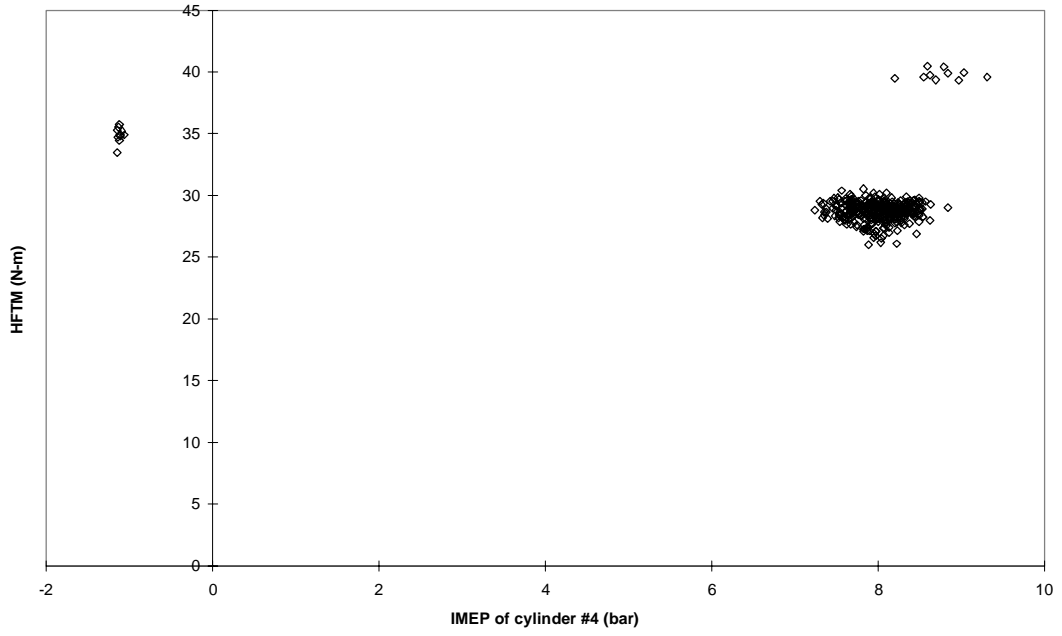


Figure B.2. LFAM versus IMEP of cylinder #4.

1200 RPM, 8.53 bar BMEP



2500 RPM, 4.85 bar BMEP

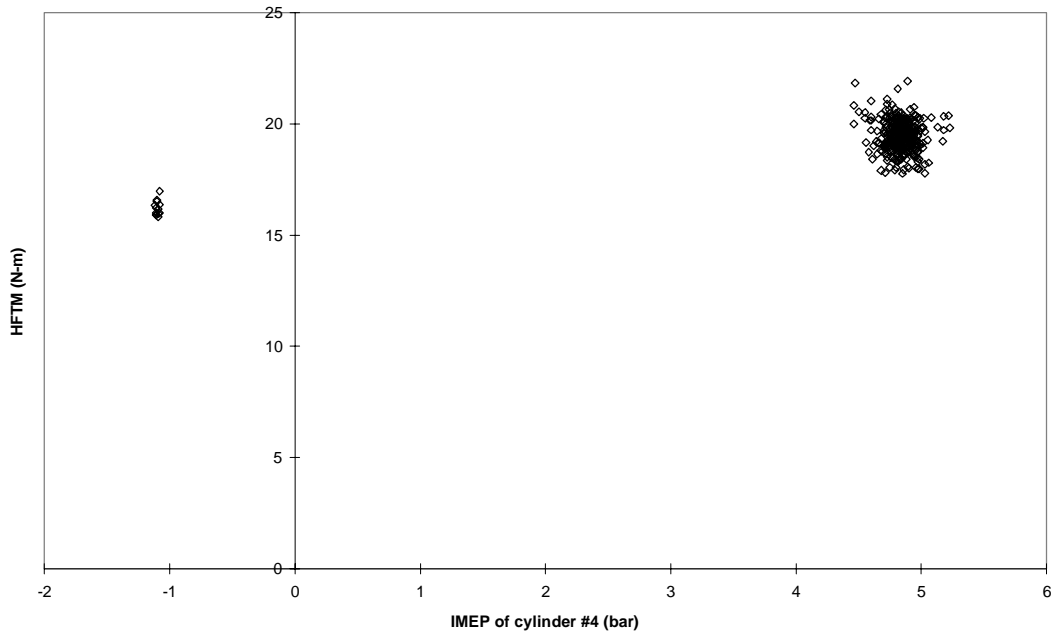


Figure B.3. HFTM versus IMEP of cylinder #4.